Surface Dual Composite Nanostructure for Improving Visible Light Absorption in Thin Silicon Films

Weishuai Chen, Jin Tao, Jinguang Lv, Yuxin Qin, Guangtong Guo, Li Qin, Jun Zhang, Jingqiu Liang, Dan Gao, and Weibiao Wang

***Abstract*—Visible light communication has attracted significant attention due to advantages such as high transmission speed, good security, high confidentiality, environmental protection, and lack of need for spectrum authorization. Herein, the problem of absorption of light in the visible band in thin silicon films is examined, and a dual composite nanostructure array based on nanoholes of two sizes is proposed to increase visible light absorption. Light absorptivity was determined to be greater than 80% at wavelengths between 400 and 678 nm. Moreover, using finite-difference time-domain numerical simulations, the distributions of the electric field at specific wavelengths were obtained, the propagation modes at these wavelengths were examined, and the effect of these modes was analyzed according to the electric field distributions. The proposed dual composite nanostructured silicon film can be used in photovoltaic devices to improve visible light absorption.**

***Index Terms*—Composite nanostructure, visible light communication, thin silicon film.**

I. Introduction

With the "great leap forward" of mobile internet data, communication technology is constantly undergoing renovation and recreation. This has ushered in a new chapter in the global information technology revolution, which has yielded novel concepts such as virtual reality, smart cities, cloud computing, and autonomous driving. While these "big data" services are rapidly developing, they also pose new challenges to the data-carrying capacity of communication networks [1]. Traditional wireless communications currently suffer from a scarcity of wireless spectrum resources. Visible light communication is a new type of communication method that employs the modulation of light with wavelengths between 400 and 800 nm to carry information. The visible light spectrum bandwidth is about 400 THz, which is significantly greater than the existing wireless communication spectrum. This extremely large bandwidth signifies that visible light communication has the potential for use in high-speed communication [2]–[6] and could greatly expand the existing wireless spectrum resources, effectively alleviating the current urgent need for wireless bandwidth. Additionally, visible light communication has many significant advantages, such as radio-frequency radiation is not produced, environmental protection, high reliability, and confidentiality [7], [8]. However, although visible light theoretically has a large communication capacity, in practice, it is limited by the materials and devices used in existing transmitters, receivers, and optical systems as well as the current digital signal processing algorithms. Therefore, increasing the rate of visible light communication systems is still challenging.

Silicon (Si) can absorb incident light in the wavelength range of 300 to 1100 nm; thus, silicon-based photodetectors are widely used in visible light communication systems. Moreover, ultrathin photodetectors could effectively improve the transmission rate of visible light communication systems. The absorption rate of a thin silicon layer in the visible light band is relatively low. Therefore, the light absorption rate of the thin silicon layer needs to be improved. For the development of ultraviolet detection, infrared detection, and solar cells, most researchers have focused on improving the absorptivity. The quantum efficiency of a detector device can be improved by including features such as plasmonic nanostructures [9]–[13], photonic crystals [14]–[16], or nanowires and nanoholes [17]–[19]. Similarly, a series of surface light trapping structures have been used to improve the performance of solar cells [20]–[32]. Furthermore, lateral and vertical detectors fabricated on silicon-on-insulator wafers

Manuscript received 30 May 2022; revised 8 July 2022; accepted 15 July 2022. Date of publication 19 July 2022; date of current version 27 July 2022. This work was supported in part by the National Key Research and Development Program under Grants 2018YFB1801902, 2018YFB1801901, and 2019YFB2006003, in part by the Jilin Province Science and Technology Development Program Project under Grant 20190302062GX, in part by the Youth Project of National Natural Science Foundation of China under Grant 12004139, and in part by the Science and Technology Plan of Guangdong Province Program Project under Grant 2016B010111003. *(Corresponding authors: Dan Gao; Weibiao Wang.)*

Weishuai Chen and Guangtong Guo are with the State Key Laboratory of Applied Optics, Changchun Institute of Optics, Fine Mechanics and Physics, Chinese Academy of Sciences, Changchun 130033, China, and also with the University of Chinese Academy of Sciences, Beijing 100049, China (e-mail: chenws159@163.com; 15563712841@163.com).

Jin Tao, Jinguang Lv, Yuxin Qin, Jingqiu Liang, Dan Gao, and Weibiao Wang are with the State Key Laboratory of Applied Optics, Changchun Institute of Optics, Fine Mechanics and Physics, Chinese Academy of Sciences, Changchun 130033, China (e-mail: taojin@ciomp.ac.cn; jinguanglv@163.com; qinyuxindavid@163.com; liangjq@ciomp.ac.cn; gx2zht@126.com; wangwb@ciomp.ac.cn).

Li Qin is with the State Key Laboratory of Luminescence and Applications, Changchun Institute of Optics, Fine Mechanics and Physics, Chinese Academy of Sciences, Changchun 130033, China (e-mail: qinl@ciomp.ac.cn).

Jun Zhang is with the Guangzhou Key Laboratory of Visible Light Communication Engineering Technology, Jinan University, Guangzhou 510632, China (e-mail: 472969511@qq.com).

This article has supplementary downloadable material available at https://doi.org/10.1109/JPHOT.2022.3192278, provided by the authors.

Digital Object Identifier 10.1109/JPHOT.2022.3192278

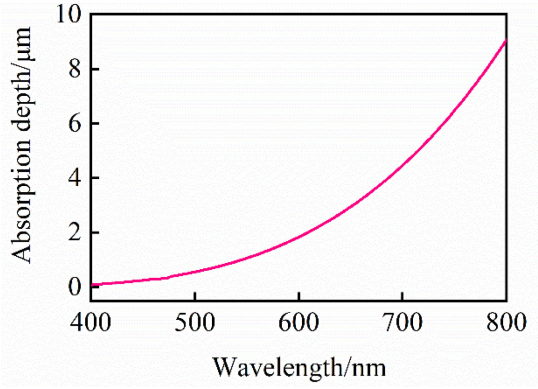

Fig. 1. Relation between the absorption depth of light in the silicon layer and the wavelength.

have been used to improve the quantum efficiency [33]–[37]. To date, few studies have been conducted relating to inorganic detectors for visible light. This study presents a design for a dual composite nanostructure in a thin silicon layer. Since this structure can enhance the absorption of visible light (400–800 nm), not only is the efficiency of the detector improved but also the range of applications for visible light communication systems is expanded and the full use of the resources of the visible spectrum is enabled.

II. Structure Design and Simulation

When light is incident on semiconductor materials, the light intensity decreases with increasing propagation distance due to the continuous occurrence of the intrinsic absorption. The absorption depth l of light in the silicon layer is usually used to represent the absorption coefficient α: $l = 1/\alpha$. The absorption coefficient is related to the imaginary part of the refractive index of the silicon material [24]. In the visible band (400–800 nm), the shorter the wavelength, the larger the imaginary part of the refractive index of silicon material and the larger the absorption coefficient, and vice versa. Fig. 1 displays the relation between the absorption depth of light and the wavelength of light in silicon (Palik's experimental measurement data were used in this report [38]). Additionally, Fig. 1 shows that the absorption depth increases with the wavelength. The absorption depth of visible light changes with the wavelength, varying from a few tenths of a micrometer to a few micrometers, and the wavelength range of red light is the widest, ranging from 608 to 800 nm, and its absorption depth in silicon is about 2–9 μm. The thickness of the silicon layer must be carefully considered in the design of a photovoltaic device. If the silicon layer is thick enough, the transmissivity of visible light will decrease and absorptivity will increase. However, when the thickness of the silicon layer is increased, the integration of devices will be affected and too much heat will be generated.

We calculated the reflectivity (R), transmissivity (T), and absorptivity (A) curves of the silicon layer with different thicknesses using the finite-difference time-domain (FDTD) method. As shown in Fig. 2(a), the calculation settings were as follows: the periodic boundary conditions were applied in the x and y directions, PML (perfectly matched layer) boundary conditions were applied in the z direction, and the plane wave was incident vertically along the negative direction of the z axis. Fig. 2(b), (c), and (d) show the variations of R, T, and A, respectively, which were calculated using the FDTD method, with varying thicknesses of the silicon layer in the visible band. As shown in Fig. 2(b)–(d), the existence of the Fabry–Perot (F–P) oscillation was obvious for the reflectivity, transmissivity, and absorptivity curves, and this phenomenon can be explained as follows: Air is present on both sides of the silicon layer, which yields a sandwich structure with a low refractive index, a high refractive index, and a low refractive index, constituting a simple F–P cavity. For the short waveband, the absorption coefficient of silicon was relatively large. When light was incident vertically, in addition to the reflected energy loss, most of the energy was absorbed in the silicon layer and no interference effects were observed. Additionally, no oscillation peaks were present in the reflectivity and transmissivity curves. For the long waveband, the extinction coefficient of silicon was small and interference effects were present, resulting in the oscillation of reflectivity and transmissivity curves. Simultaneously, for the long wavelength band, as the thickness of the silicon layer increased, most of the energy was absorbed in the silicon layer and the interference effect gradually weakened. This caused the gradual weakening of the oscillations of the reflectivity and transmittance curves. Fig. 2(d) also shows that, when the thickness of silicon was less than 10 μm, the optical absorptivity of Si in the visible band exhibited an upward trend with increasing thickness, and when the thickness of the silicon layer was greater than 10 μm, the thickness of the silicon layer was greater than the absorption depth of the red band (Fig. 1) and the absorptivity exhibits little change. For the short band of visible light, the high reflectivity of the silicon surface affects the absorptivity of the silicon layer. For the long band of visible light, the absorptivity depends on the thickness of the silicon layer. However, if the silicon layer is too thick, difficulties will arise during device integration and other photoelectric properties of the device will be affected.

To improve the absorptivity of visible light in a thin silicon layer, a dual composite nanohole array (DCN-A) based on nanoholes of two different sizes was designed on the silicon surface. Fig. 3(a) displays the schematic of Si/DCN-A, and Fig. 3(b) shows its cross-sectional diagram. As shown in Fig. 3(a), h_2 is the thickness of the silicon layer; r_1 is the radius of the smaller sized nanohole, r_2 is the radius of the larger sized nanohole, and $r_2 = 2r_1$; p_1 is the period of the smaller sized nanohole, p_2 is the period of the larger sized nanohole, and $p_2 = 2p_1$; p is the period of Si/DCN-A and $p = 2p_2 = 4p_1$; and d is the depth of Si/DCN-A. A SiO_2 layer with a thickness of h_1 is present below the silicon layer. The effect of DCN-A on the light absorption of the silicon layer was determined using the FDTD method in the visible light band. The calculation settings were as follows: the periodic boundary conditions were applied in the x and y directions; the plane wave propagated in the z direction; and the wavelength range was 400–800 nm. Additionally, the polarization direction of the electric field was along the x-axis. A perfectly matched

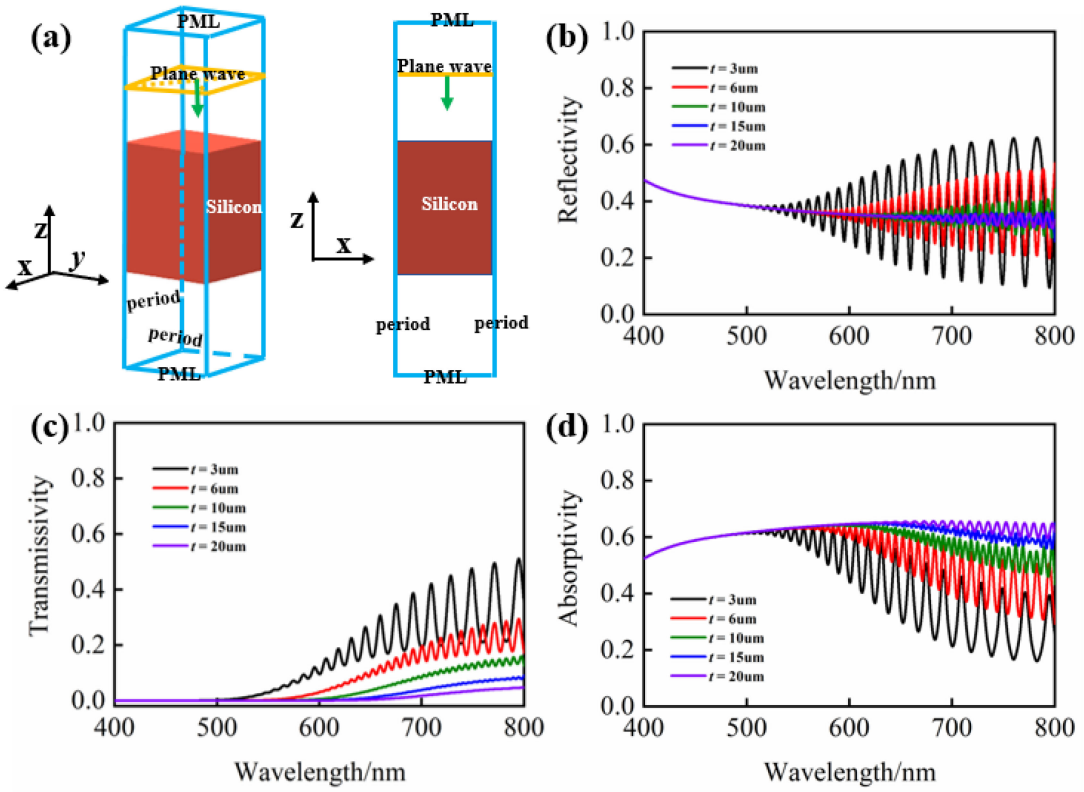

Fig. 2. (a) Schematic of calculation settings; (b) Relation between reflectivity and thickness of the silicon layer; (c) Relation between transmissivity and thickness of the silicon layer; (d) Relation between absorptivity and thickness of the silicon layer. The black solid line represents $t = 3$ μm, the red line represents $t = 6$ μm, the green line represents $t = 10$ μm, the blue line represents $t = 15$ μm, and the purple line represents $t = 20$ μm.

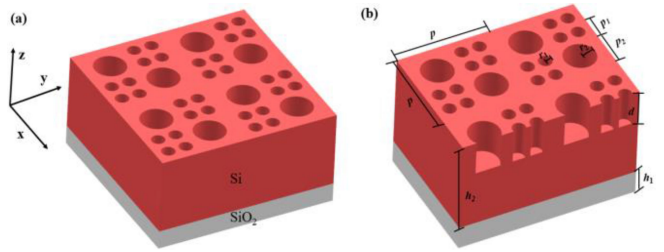

Fig. 3. (a) Schematic of the composite nanostructure; (b) Cross-sectional diagram of the composite nanostructure.

layer was used to absorb any reflection and transmission fields along the z direction.

III. Results and Discussion

We used $A = 1 - T - R$ to determine the light absorption of the thin silicon layer, where R and T were obtained from the FDTD numerical simulation. R and T are factors that directly affect the absorptivity of visible light in the silicon layer, and DCN-A can modulate the R and T of a silicon film layer. We set the thickness of the silicon layer as $h_2 = 3$ μm and that of the SiO_2 layer as $h_1 = 500$ nm. To achieve high visible light absorptivity in the thin silicon layer, the effect of DCN-A with different structure parameters on silicon layer absorptivity was calculated using FDTD.

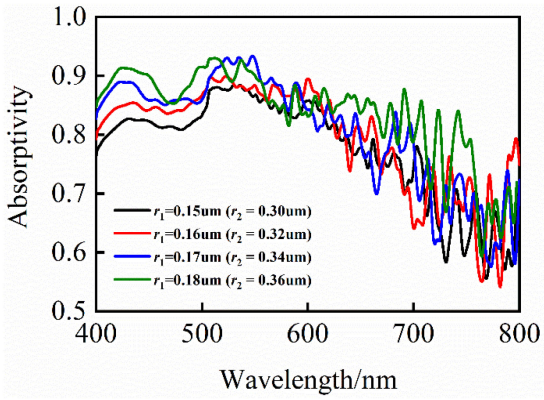

Fig. 4. Light absorptivity curve of Si/DCN-A with $p = 1.6$ μm, $d = 1.0$ μm, and $r_1 = 0.15$, 0.16, 0.17, or 0.18 μm. The black solid line represents the nanohole radius $r_1 = 0.15$ μm and $r_2 = 0.30$ μm, the red line represents $r_1 = 0.16$ μm and $r_2 = 0.32$ μm, the blue line represents $r_1 = 0.17$ μm and $r_2 = 0.34$ μm, and the green line represents $r_1 = 0.18$ μm and $r_2 = 0.36$ μm.

Fig. 4 displays the relation between the absorptivity curve and wavelength with different nanohole radii. The period of DCN-A was fixed at $p = 1.6$ μm ($p_1 = 0.4$ μm, $p_2 = 0.8$ μm), the depth was fixed at $d = 1.0$ μm, the radius of the smaller sized nanohole r_1 was set as 0.15, 0.16, 0.17, or 0.18 μm, and the radius of the larger sized nanohole r_2 was set as 0.30, 0.32, 0.34, or 0.36 μm. The light absorptivity curves calculated using the FDTD method are shown in Fig. 4. The figure shows that

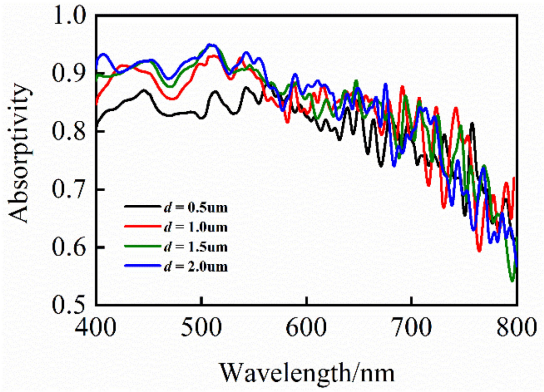

Fig. 5. Light absorptivity curves of Si/DCN-A with $p = 1.6$ μm, $r_1 = 0.18$ μm, $r_2 = 0.36$ μm, and $d = 0.5$, 1.0, 1.5, or 2.0 μm. The black solid line represents the DCN-A depth $d = 0.5$ μm, the red line represents $d = 1.0$ μm, the green line represents $d = 1.5$ μm, and the blue line represents $d = 2.0$ μm.

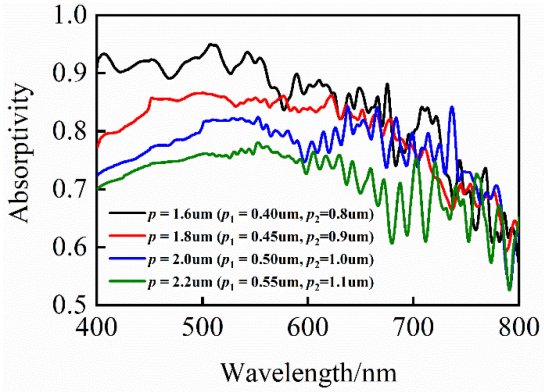

Fig. 6. Light absorptivity curves of Si/DCN-A with $r_1 = 0.18$ μm, $r_2 = 0.36$ μm, $d = 2.0$ μm, and $p = 1.6$, 1.8, 2.0, or 2.2 μm. The black solid line represents the period of nanocomposite structure $p = 1.6$ μm, the red line represents $p = 1.8$ μm, the blue line represents $p = 2.0$ μm, and the green line represents $p = 2.2$ μm.

when the period and depth were fixed, the absorptivity curve for 400–800 nm exhibited an upward trend with increasing radii. As shown in the figure, the absorptivity in small wavelengths of light between 400–500 nm is improved by increasing the radius of holes is obviously, this phenomenon can be explained as follows: Si has high surface reflectivity and large absorption coefficient in small wavelength of light. When the period and depth of the nanohole arrays are fixed, with the increase of the radius of the nanohole, the surface reflection area decreases and the absorption area of the incident light of the nanohole increases. In addition, compared with the short wave visible light band, the light absorptivity curve in the long visible light band sharply fluctuated. When $r_1 = 0.18$ μm and $r_2 = 0.36$ nm, the light absorptivity in the visible band was relatively high.

Fig. 5 displays the relation between absorptivity curve and wavelength with varying DCN-A depth. The period of DCN-A was fixed at $p = 1.6$ μm ($p_1 = 0.4$ μm, $p_2 = 0.8$ μm), the radius of the smaller sized nanohole was fixed at $r_1 = 0.18$ μm, the radius of the larger sized nanohole was fixed at $r_2 = 0.36$ μm, and the depth of DCN-A was set as 0.5, 1.0, 1.5 or 2.0 μm. The light absorptivity curves calculated using the FDTD method are shown in Fig. 5. The figure shows that for the blue light band with a wavelength of 400–500 nm, the light absorptivity curve exhibited an upward trend with increasing d. When $d \geq 1$ μm, the change of light absorptivity curve with the DCN-A depth was relatively small for incident light with wavelengths greater than 626 nm. Thus, the absorptivity in the short band of visible light can be effectively improved by increasing d.

Fig. 6 displays the relation between the absorptivity curve and wavelength with different DCN-A periods. The radius of the smaller sized nanohole was fixed at $r_1 = 0.18$ μm, and the radius of the larger sized nanohole was fixed at $r_2 = 0.36$ μm. The depth was fixed at $d = 2.0$ μm, and the period of DCN-A was set as $p =$ 1.6, 1.8, 2.0, or 2.2 μm. The light absorptivity curves calculated using the FDTD method are shown in Fig. 5. The figure shows that for λ between 400 and 500 nm, the absorptivity decreased with increasing DCN-A period. Compared with that in the long visible band, the light absorptivity in the short visible band was more sensitive to the change of period. When $p = 1.6$ μm, the light absorptivity was higher in the bands of 400–573, 581–623, 636–678, 700–726, 740–744, and 763–771 nm, covering most of the visible band.

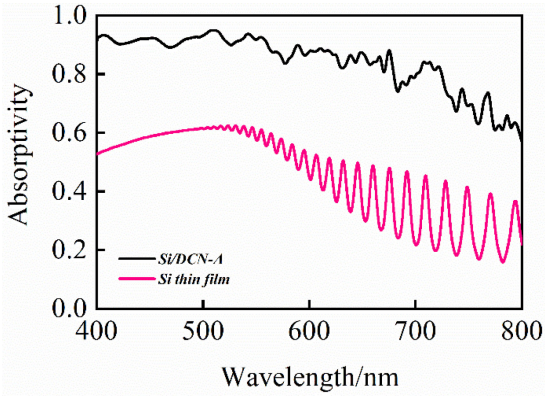

Fig. 7. Light absorptivity curves of Si/DCN-A with $r_1 = 0.18$ μm, $r_2 = 0.36$ μm, $d = 2.0$ μm, and $p = 1.6$ μm ($p_1 = 0.4$ μm, $p_2 = 0.8$ μm).

Based on the above research and after repeated optimization, the following structural parameters of DCN-A were chosen: $r_1 =$ 0.18 μm, $r_2 = 0.36$ μm, $d = 2.0$ μm, and $p = 1.6$ μm ($p_1 =$ 0.4 μm, $p_2 = 0.8$ μm). Fig. 7 compares the absorptivity curves of Si/DCN-A (shown by a black solid line in the figure) and those of the Si thin film (shown by the pink solid line in the figure) in the visible light band. According to the black solid line in Fig. 7, for wavelengths λ between 400 and 626 nm, the optical absorptivity of Si/DCN-A was greater than 0.85; for λ between 626 and 678 nm, the absorptivity of Si/DCN-A was greater than 0.80; for λ between 678 and 698 nm, the absorptivity of Si/DCN-A was greater than 0.75; for λ between 698 and 735 nm, the absorptivity of Si/DCN-A was greater than 0.70; and for λ between 735 and 797 nm, the absorptivity of Si/DCN-A was greater than 0.60. Thus, DCN-A can effectively improve the light absorptivity of Si thin films in the visible band. The fundamental Bloch, channeling Bloch, and guided resonance modes are the main modes excited by DCN-A in the visible light band [39], [40]. DCN-A supports the fundamental Bloch modes

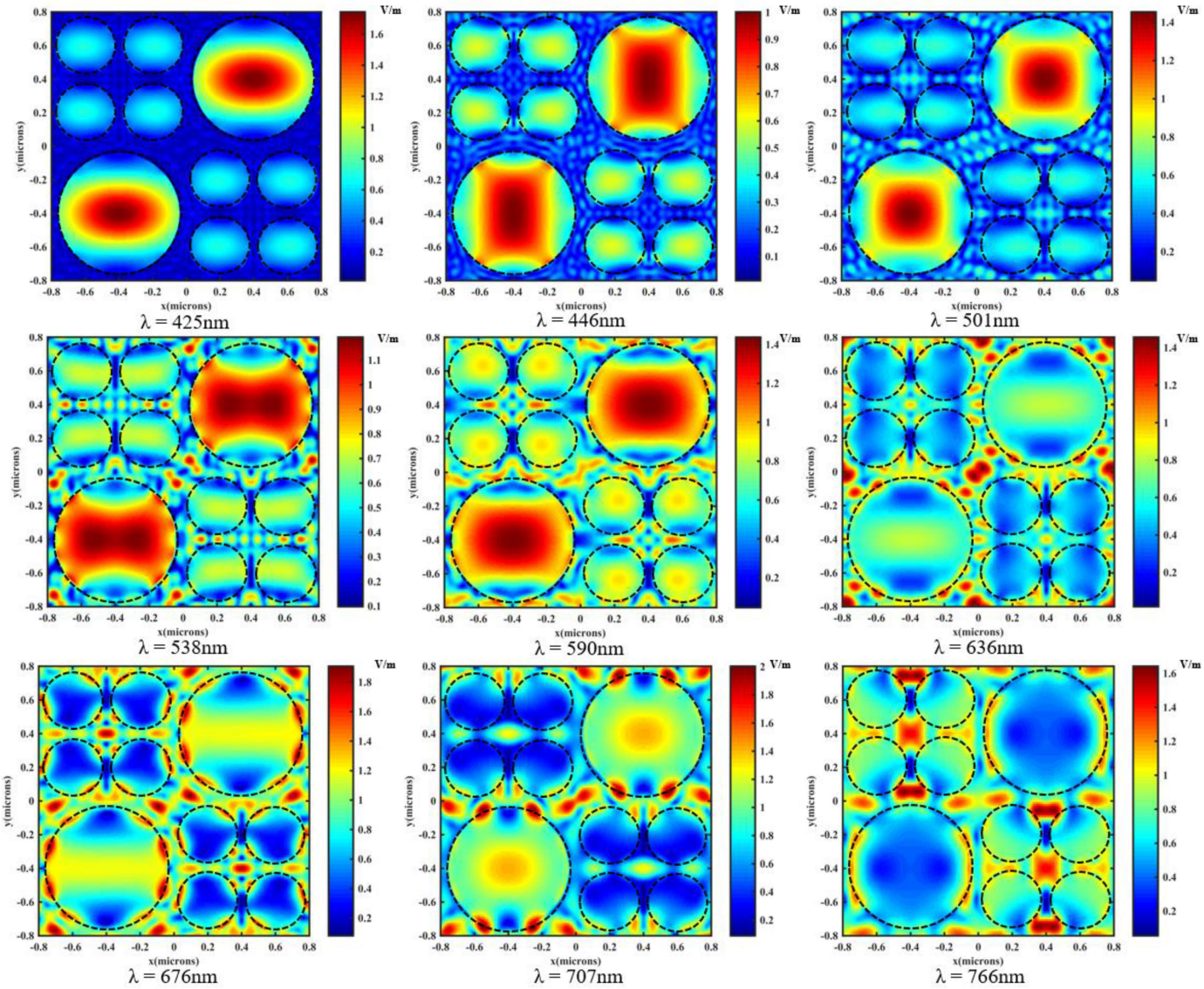

Fig. 8. The *x*–*y* plane the electric field distributions at λ = 425, 446, 501, 538, 590, 636, 676, 707, and 766 nm. (The electric field intensity of the incident light: *E*= 1 V/m.).

of all incident waves in the 400–800 nm band; when the channel mode is excited, the field strength is mainly concentrated in the nanoholes [40]. Furthermore, the field strength distribution of the guided resonance mode is mainly concentrated in the sidewall of the nanoholes, and the excitation of this mode is usually accompanied by violent fluctuations in absorptivity, which yields numerous resonance peaks with narrow half-widths and random intervals [41]–[44]. As shown by the black solid line in Fig. 7, for 400 nm $< \lambda <$ 510 nm, the light absorptivity curve was relatively smooth, and the channel mode was the main mode excited by the DCN-A in this band. For 510 nm $< \lambda <$ 636 nm, the absorptivity curve displayed obvious fluctuations, the DCN-A excited the channel mode and guided wave resonance mode in this band, and the channel mode remained the main excitation mode in this band. For $\lambda >$ 636 nm, the light absorptivity curve sharply fluctuated and the guided wave resonance mode was the main excitation mode of DCN-A in this band.

To further examine the effect of DCN-A on optical absorptivity, we calculated the electric field distributions at λ = 425, 446, 501, 538, 590, 636, 676, 707, and 766 nm; the field strength distributions are shown in Fig. 8. The figure shows that in the *x*–*y* plane, the intensities at λ = 425, 466, and 501 nm were mainly concentrated in the nanoholes, indicating that channeling modes are the main mode of optical propagation. At λ = 538 and 590 nm, although a small part of the field intensities was concentrated in the sidewall of the nanoholes, most of the field intensities was concentrated in the nanoholes and the channeling modes remained the main modes of optical propagation. At λ = 636, 676, 707, and 766 nm, the electric field intensity was concentrated at the sidewall of the nanoholes, signifying that the guided resonance modes are the main modes of optical propagation.

Fig. 9 compares the light absorptivity curves of Si/small-sized nanohole array (structural parameters: r_1 = 0.18 μm, d =

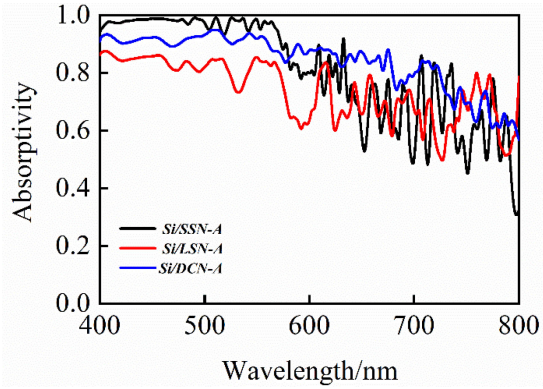

Fig. 9. Comparison of the absorptivity curves of Si/SSN-A, Si/LSN-A, and Si/DCN-A in the visible light band. The black, red, and blue solid lines represent the absorptivity curve of Si/SSN-A, Si/LSN-A, and Si/DCN-A, respectively.

2 μm, and $p_1 = 0.4$ μm, shown by the black solid line in the figure), large-sized nanohole array (structural parameters: $r_2 = 0.36$ μm, $d = 2$ μm, and $p_2 = 0.8$ μm, shown by the solid red line in the figure), and Si/DCN-A (shown by the solid blue line in the figure) in the visible light band. The figure shows that for the Si/small-sized nanohole arrays (Si/SSN-A), the light absorptivity was relatively high in the range of 400–584 nm, and in the range of 604–800 nm, due to the excitation of the guided resonance mode, the optical absorptivity sharply fluctuated and a large number of resonance peaks were obtained. For the Si/large-sized nanohole arrays (Si/LSN-A), in the range of 400–611 nm, the light absorptivity was always lower than that of Si/SSN-A, and in the range of 611–800 nm, compared with Si/SSN-A, fewer guided resonance peaks were afforded. For Si/DCN-A, in the range of 400–584 nm, the optical absorptivity was smaller than that of Si/SSN-A, but the light absorptivity still exceeded 0.83 in this range. In the range of 584–800 nm, compared with Si/SSN-A and Si/LSN-A, Si/DCN-A exhibited higher light absorptivity while affording fewer guided resonance peaks and its light absorptivity curve was relatively smooth.

IV. Conclusion

To improve the absorption rate of visible light in a thin silicon layer, a dual composite nanostructure based on nanoholes of two different sizes was designed on a silicon surface. The proposed Si/DCN-A exhibited light absorptivity exceeding 0.8 for wavelengths between 400 and 678 nm. This study also showed that in the visible light band, periodically arranged DCN-A in a silicon layer can improve light absorptivity through the combined action of three light propagation modes. Finally, we compared the light absorptivity of Si/DCN-A, Si/LSN-A, and Si/SSN-A in the visible light band. Compared to the single-sized nanohole arrays, the DCN-A exhibits a better absorptivity enhancement effect over the whole visible band. The results of this study provide a reference for the design of other photovoltaic devices.

Appendix

See Appendix 1 for the supporting content.

References

[1] L. E. M. Matheus, A. B. Vieira, L. F. M. Vieira, M. A. M. Vieira, and O. Gnawali, "Visible light communication: Concepts, applications and challenges," *IEEE Commun. Surv. Tut.*, vol. 21, no. 4, pp. 3204–3237, Oct.–Dec. 2019, doi: 10.1109/COMST.2019.2913348.

[2] L. U. Khan, "Visible light communication: Applications, architecture, standardization and research challenges," *Digit. Commun. Netw.*, vol. 3, no. 2, pp. 78–88, 2017, doi: 10.1016/j.dcan.2016.07.004.

[3] M. Seminara, M. Meucci, F. Tarani, C. Riminesi, and J. Catani, "Characterization of a VLC system in real museum scenario using diffusive LED lighting of artworks," *Photon. Res.*, vol. 9, no. 4, pp. 548–557, 2021, doi: 10.1364/PRJ.414394.

[4] A. Minotto *et al.*, "Visible light communication with efficient far-red/near-infrared polymer light-emitting diodes," *Light: Sci. Appl.*, vol. 9, no. 1, pp. 1–11, 2020, doi: 10.1038/s41377-020-0314-z.

[5] M. Portnoi *et al.*, "Bandwidth limits of luminescent solar concentrators as detectors in free-space optical communication systems," *Light: Sci. Appl.*, vol. 10, no. 1, pp. 1–12, 2021, doi: 10.1038/s41377-020-00444-y.

[6] I. Tavakkolnia *et al.*, "Organic photovoltaics for simultaneous energy harvesting and high-speed MIMO optical wireless communications," *Light: Sci. Appl.*, vol. 10, no. 1, pp. 1–11, 2021, doi: 10.1038/s41377-021-00487-9.

[7] H. Sadat, M. Abaza, A. Mansour, and A. Alfalou, "A survey of NOMA for VLC systems: Research challenges and future trends," *Sensors*, vol. 22, no. 4, 2022, Art. no. 1395, doi: 10.3390/s22041395.

[8] S. U. Rehman *et al.*, "Visible light communication: A system perspective—Overview and challenges," *Sensors*, vol. 19, no. 5, 2019, Art. no. 1153, doi: 10.3390/s19051153.

[9] O. L. Muskens, V. Giannini, J. A. Sánchez-Gil, and J. G. Rivas, "Strong enhancement of the radiative decay rate of emitters by single plasmonic nanoantennas," *Nano Lett.*, vol. 9, no. 7, pp. 2871–2875, Aug. 2007, doi: 10.1021/nl0715847.

[10] S. A. Maier, P. G. Kik, and H. A. Atwater, "Observation of coupled plasmon-polariton modes in Au nanoparticle chain waveguides of different lengths: Estimation of waveguide loss," *Appl. Phys. Lett.*, vol. 81, no. 9, pp. 1714–1716, Aug. 2002, doi: 10.1063/1.1503870.

[11] J. Hendrickson, J. Guo, and W. Kim, "Subwavelength metal grating metamaterial for polariza-tion-selective optical antireflection coating," *J. Opt. Soc. Amer. B*, vol. 32, no. 7, pp. 1392–1398, Jul. 2015, doi: 10.1364/JOSAB.32.001392.

[12] D. M. Nguyen, D. Lee, and J. Rho, "Control of light absorbance using plasmonic grating based perfect absorber at visible and near-infrared wavelengths," *Sci. Rep.*, vol. 7, Jun. 2017, Art. no. 2611, doi: 10.1038/s41598-017-02847-1.

[13] J. Wang, Y. Chen, X. Chen, J. Hao, M. Yan, and M. Qiu, "Photothermal reshaping of gold nanoparticles in a plasmonic absorber," *Opt. Exp.*, vol. 19, no. 15, pp. 14726–14734, Jul. 2011. doi: 10.1364/OE.19.014726.

[14] H. Shigeta *et al.*, "Enhancement of photocurrent in ultrathin active-layer photodetecting devices with photonic crystals," *Appl. Phys. Lett.*, vol. 101, Oct. 2012, Art. no. 161103, doi: 10.1063/1.4759149.

[15] Y. Tanaka, Y. Kawamoto, M. Fujita, and S. Noda, "Enhancement of broadband optical absorption in photovoltaic devices by band-edge effect of photonic crystals," *Opt. Exp.*, vol. 21, pp. 20111–20118, 2013, doi: 10.1364/OE.21.020111.

[16] K. Zang *et al.*, "Silicon single-photon avalanche diodes with nano-structured light trapping," *Nature Commun.*, vol. 8, no. 1, pp. 1–6, 2017. doi: 10.1038/s41467-017-00733-y.

[17] Y. Gao *et al.*, "Photon-trapping microstructures enable high speed high-efficiency silicon photodiodes," *Nature Photon.*, vol. 11, no. 5, pp. 301–308, 2017, doi: 10.1038/nphoton.2017.37.

[18] C. Bartolo-Perez *et al.*, "Avalanche photodetectors with photon trapping structures for biomedical imaging applications," *Opt. Exp.*, vol. 29, no. 12, pp. 19024–19033, 2021, doi: 10.1364/OE.421857.

[19] A. Zhang, H. Kim, J. Cheng, and Y.-H. Lo, "Ultrahigh responsivity visible and infrared detection using silicon nanowire phototransistors," *Nano Lett.*, vol. 10, no. 6, pp. 2117–2120, May 2010, doi: 10.1021/nl1006432.

[20] M. D. Kelzenberg *et al.*, "Enhanced absorption and carrier collection in Si wire arrays for photovoltaic applications," *Natute Mater.*, vol. 9, pp. 239–244, Feb. 2010, doi: 10.1038/nmat2727.

[21] Y. Park *et al.*, "Absorption enhancement using photonic crystals for silicon thin film solar cells," *Opt. Exp.*, vol. 17, no. 16, pp. 14312–14321, Aug. 2009, doi: 10.1364/OE.17.014312.

[22] E. Garnett and P. Yang, "Light trapping in silicon nanowire solar cells," *Nano Lett.*, vol. 10, no. 3, pp. 1082–1087, Jan. 2010, doi: 10.1021/nl100161z.

[23] Y. Wu, Z. Xia, Z. Liang, Z. Jian, and X. Qin, "Broadband absorption enhancement in elliptical silicon nanowire arrays for photovoltaic applications," *Opt. Exp.*, vol. 22, no. Suppl. 5, 2014, Art. no. A1292, doi: 10.1364/OE.22.0A1292.

[24] S. E. Han and G. Chen, "Optical absorption enhancement in silicon nanohole arrays for solar photovoltaics," *Nano Lett.*, vol. 10, pp. 1012–1015, Feb. 2010, doi: 10.1021/nl904187m.

[25] M. A. Shameli and L. Yousefi, "Absorption enhanced thin-film solar cells using fractal nano-structures," *IET Optoelectron.*, vol. 15, no. 5, pp. 248–253, Mar. 2021, doi: 10.1049/ote2.12036.

[26] H. Heidarzadeh and H. Bahador, "Photocurrent improvement of an ultra-thin silicon solar cell using cascaded cylindrical shape plasmonic nanoparticles," *Physica Scripta*, vol. 96, no. 5, Feb. 2021, Art. no. 055501, doi: 10.1088/1402-4896/abe585.

[27] Z. Durmaz, S. Husein, and R. Saive, "Thin silicon interference solar cells for targeted or broadband wavelength absorption enhancement," *Opt. Exp.*, vol. 29, no. 3, pp. 4324–4337, 2021, doi: 10.1364/OE.413294.

[28] Z. Yu, A. Raman, and S. Fan, "Fundamental limit of nanophotonic light-trapping in solar cells," *Proc. Nat. Acad. Sci.*, vol. 107, no. 41, pp. 17491–17496, Oct. 2010, doi: 10.1073/pnas.10082961.

[29] E. Yablonovitch, "Statistical ray optics," *J. Opt. Soc. Amer.*, vol. 72, no. 7, pp. 899–907, 1982, doi: 10.1364/JOSA.72.000899.

[30] G. Marko, A. Prajapati, and G. Shalev, "Subwavelength nonimaging light concentrators for the harvesting of the solar radiation," *Nano Energy*, vol. 61, pp. 275–283, Jul. 2019, doi: 10.1016/j.nanoen.2019.04.082.

[31] D. M. Callahan, J. N. Munday, and H. A. Atwater, "Solar cell light trapping beyond the ray optic limit," *Nano Lett.*, vol. 12, no. 1, pp. 214–218, Dec. 2012, doi: 10.1021/nl203351k.

[32] J. Oh, H. C. Yuan, and H. M. Branz, "An 18.2%-efficient black-silicon solar cell achieved through control of carrier recombination in nanostructures," *Nature Nanotechnol.*, vol. 7, pp. 743–748, 2012, doi: 10.1038/NNANO.2012.166.

[33] A. Afzalian and D. Flandre, "Measurements, modeling and electrical simulations of lateral PIN photodiodes in thin film-SOI for high quantum efficiency and high selectivity in the UV range," in *Proc. 33rd Conf. Eur. Solid State Device Res.*, 2003, pp. 55–58, doi: 10.1109/ESSDERC.2003.1256809.

[34] A. Afzalian and D. Flandre, "Physical modeling and design of thin-film SOI lateral PIN photodiodes," *IEEE Trans. Electron. Devices*, vol. 52, no. 6, pp. 1116–1122, Jun. 2005, doi: 10.1109/ted.2005.848080.

[35] A. Afzalian and D. Flandre, "Monolithically integrated 10 Gb/s photodiode and transimpedance amplifier in thin-film SOI CMOS technology," *Electron. Lett.*, vol. 42, no. 24, pp. 1420–1421, Nov. 2006, doi: 10.1049/el:20062563.

[36] A. Afzalian and D. Flandre, "Seed performances of thin-film lateral SOI PIN photodiodes up to tens of GHz," in *Proc. IEEE Int. SOI Conf.*, 2006, pp. 83–84, doi: 10.1109/SOI.2006.284444.

[37] A. Afzalian and D. Flandre, "Characterization of quantum efficiency, effective lifetime and mo-bility in thin film ungated SOI lateral PIN photodiodes," *Solid State Electron.*, vol. 51, no. 2, pp. 337–342, Feb. 2007, doi: 10.1016/j.sse.2007.01.009.

[38] E. D. Palik, *Handbook of Optical Constants of Solids*. New York, NY, USA; Orlando, FL, USA; San Diego, CA, USA: Academic, 1985.

[39] D. Gao, J. Zhang, F. Wang, J. Q. Liang, and W. B. Wang, "Design and simulation of ultra-thin and high-efficiency silicon-based trichromatic PIN photodiode arrays for visible light communication," *Opt. Commun.*, vol. 475, 2020, Art. no. 126296, doi: 10.1364/OFC.2015.Tu2G.5.

[40] J. L. Donnelly *et al.*, "Mode-based analysis of silicon nanohole arrays for photovoltaic applications," *Opt. Exp.*, vol. 22, no. Suppl. 5, 2014, Art. no. A1343, doi: 10.1364/OE.22.0A1343.

[41] Q. G. Du, H. K. Chan, H. V. Demir, Y. Y. Hong, and X. W. Sun, "Enhanced optical absorption in nanopatterned silicon thin films with a nano-cone-hole structure for photovoltaic applications," *Opt. Lett.*, vol. 36, pp. 1713–1715, 2011, doi: 10.1364/OL.36.001713.

[42] B. Sturmberg, K. B. Dossou, L. C. Botten, A. A. Asatryan, and R. C. McPhedran, "Modal analysis of enhanced absorption in silicon nanowire arrays," *Opt. Exp.*, vol. 19, no. Suppl. 5, pp. A1067–A1081, 2011, doi: 10.1364/OE.19.0A1067.

[43] W. Chen *et al.*, "Surface silicon nanostructure for enhancement of blue light absorption," *Results Phys.*, vol. 32, 2022, Art. no. 105133, doi: 10.1016/j.rinp.2021.105133.

[44] S. Fan and J. D. Joannopoulos, "Analysis of guided resonances in photonic crystal slabs," *Phys. Rev. B*, vol. 65, 2002, Art. no. 235112, doi: 10.1103/PhysRevB.65.235112.